Nuclear Engineering and Technology 53 (2021) 2334–2340

Contents lists available at ScienceDirect

Nuclear Engineering and Technology

journal homepage: www.elsevier.com/locate/net

Original Article

A novel radioactive particle tracking algorithm based on deep rectifier neural network

Roos Sophia de Freitas Dam [a, b, *], Marcelo Carvalho dos Santos [a], Filipe Santana Moreira do Desterro [a], William Luna Salgado [a, b], Roberto Schirru [a], César Marques Salgado [b]

[a] Universidade Federal do Rio de Janeiro, Programa de Engenharia Nuclear (UFRJ / PEN), Avenida Horácio Macedo, 2030, Bloco G - Sala 206, Zip Code 21941-914, Cidade Universitária, RJ, Brazil
[b] Instituto de Engenharia Nuclear (IEN), Rua Hélio de Almeida, 75, Zip Code 21941-906, Cidade Universitária, RJ, Brazil

ARTICLE INFO

Article history:
Received 18 August 2020
Received in revised form
17 November 2020
Accepted 4 January 2021
Available online 8 January 2021

Keywords:
Radioactive particle tracking
Gamma densitometry
MCNPX code
Deep learning
Deep neural networks

ABSTRACT

Radioactive particle tracking (RPT) is a minimally invasive nuclear technique that tracks a radioactive particle inside a volume of interest by means of a mathematical location algorithm. During the past decades, many algorithms have been developed including ones based on artificial intelligence techniques. In this study, RPT technique is applied in a simulated test section that employs a simplified mixer filled with concrete, six scintillator detectors and a ^{137}Cs radioactive particle emitting gamma rays of 662 keV. The test section was developed using MCNPX code, which is a mathematical code based on Monte Carlo simulation, and 3516 different radioactive particle positions (x,y,z) were simulated. Novelty of this paper is the use of a location algorithm based on a deep learning model, more specifically a 6-layers deep rectifier neural network (DRNN), in which hyperparameters were defined using a Bayesian optimization method. DRNN is a type of deep feedforward neural network that substitutes the usual sigmoid based activation functions, traditionally used in vanilla Multilayer Perceptron Networks, for rectified activation functions. Results show the great accuracy of the DRNN in a RPT tracking system. Root mean squared error for x, y and coordinates of the radioactive particle is, respectively, 0.03064, 0.02523 and 0.07653.

1. Introduction

Nuclear techniques based on gamma densitometry are minimally invasive and do not need to interrupt operational plant conditions. These techniques are widely used in several areas such as: volume fraction calculations [1]; flow measurements [2–8]; monitoring petroleum by-products [9,10]; and density prediction [11–13]. Therefore, radioactive particle tracking (RPT) is a nuclear technique that has been used for many years with different purposes. RPT is based on tracking a radioactive particle that emits gamma radiation inside a recipient of interest, which is filled with certain materials (gas, liquid or solid flows). In order to track the radioactive particle, it is necessary to have an array of detectors and a location algorithm. RPT systems allow the study of fluidized beds [14–17], bubble columns reactors [18–22], conical spouted bed [23], concrete mixers [24,25], among others.

The RPT detection system depends on some factors, in which it is possible to highlight: gamma ray and source activity; interaction of gamma ray with matter (Compton scattering, photoelectric absorption); solid angle of the detector; detection efficiency; photopeak fraction and dead time [26]. In addition, the performance of a RPT system is directly related to the characteristics of the radionuclide chosen as a radioactive particle, such as: purity; activity; half-life; and gamma ray energy [26]. Therefore, the choice of the radionuclide is of great importance. Some of the radionuclides reported in the literature are ^{46}Sc (889.28 keV and 1120.54 keV) [15,16,19,21] and ^{198}Au (411.80 keV) [16].

Moreover, to track que radioactive particle, the RPT location algorithm converts the detector counts as a function of the

* Corresponding author. , Universidade Federal do Rio de Janeiro, Programa de Engenharia Nuclear (UFRJ / PEN), Avenida Horácio Macedo, 2030, Bloco G - Sala 206, Zip Code 21941-914, Cidade Universitária, RJ, Brazil.
E-mail addresses: rdam@coppe.ufrj.br (R.S.F. Dam), jovitamarcelo@gmail.com (M.C. dos Santos), filipe@lmp.ufrj.br (F.S.M. do Desterro), wlsalgado@con.ufrj.br (W.L. Salgado), schirru@lmp.ufrj.br (R. Schirru), otero@ien.gov.br (C.M. Salgado).

https://doi.org/10.1016/j.net.2021.01.002

radioactive particle coordinates (x, y, z). Over the last few decades, many traditional location algorithms have been developed [14,15,17,18,27–29]. In addition, the development of algorithms based on artificial intelligence (AI) techniques have also been explored [16,22,24,25].

AI techniques, such as artificial neural networks (ANN), have been used in different fields of research. The use of ANN makes it possible to study multiphase reactors [16], volume fractions [30–34], inorganic scale in oil pipelines [35], fluid density [12,13,36], predict radiation dose [37], predict radioactive particle position [22,24,25].

In a great part of these studies, ANN models with few internal processing layers or few processing units were utilized. Therefore, as presented in the literature [38,39], although these ANN models presented satisfactory results in some of these studies, in robust problems with extensive datasets, the ANN models tend to present inferior learning and generalization capability than more elaborated ANN models, which nowadays are called deep learning (DL) models. These DL models are deep neural networks (DNNs) architectures that contain multiple internal processing layers with hundreds or thousands of processing units. Especially in more complex problems, the DNNs performance stands out in comparison with the simple ANNs, where a large dataset, with thousands of examples, is necessary to cover the entire search space of the problem.

Although the DNNs have superior performance in more complex problems, for a long time the use was limited due to factors as: small quantity of data to train the models, limited hardware processing capacity to run the models and DNN architectures with inference training capacity. However, in the last decade these barriers were overcome, due to the large amount of easily accessible data available now, the use of parallel computing based on Graphic Processor Units (GPUs) to train the models, and the new more efficient DNN architectures. Therefore, in the recent years, DL models have been used to solve problems of pattern recognition with greater accuracy and faster training time. In such a way, studies in the nuclear field are already using DNNs in order to inspect structural components of nuclear power plants (NPPs) [40], analysis of reactor cores perturbation [41], detect fault/anomalies in NPPs [42], predict radiation dose [43] and identify accidents in NPPs [44,45].

Based on this, the study here presented proposes a simulated test section that consists of a mixer filled with concrete that is made with Portland cement, six NaI(Tl) scintillator detectors and a ^{137}Cs (662 keV) radioactive particle with isotropic emission of gamma rays. In previous research, R.S.F. Dam et al. (2019) proposed the use of a simple feed-forward ANN architecture, more specifically a Multilayer Perceptron (MLP) activated with sigmoid functions, as a location algorithm and used a dataset with 108 patterns to train and test the neural network [24]. The novelty of the present study is the use of a DL model, more specifically deep rectifier neural network (DRNN) [46], as a location algorithm, and the use of a dataset with 3516 patterns to train and test the DRNN, in order to improve precision in RPT technique. The simulated model was developed using MCNPX code [47] in order to generate data to feed the DRNN.

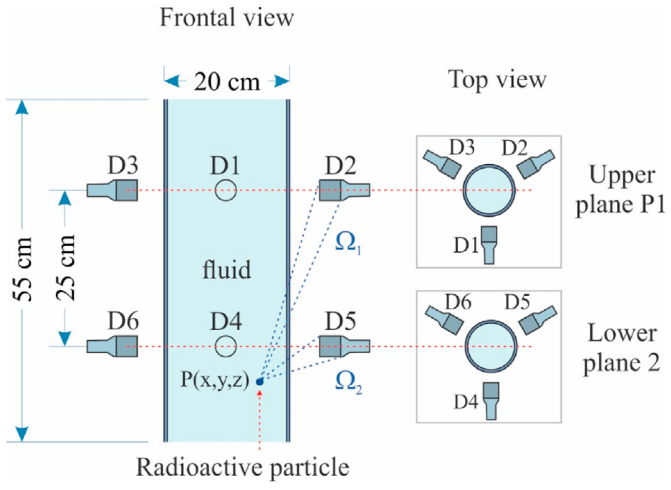

Fig. 1. Representation of the RPT simulated system.

2. The deep artificial neural network architecture

Artificial neural networks are mathematical models originally inspired by the functioning of the human brain, in which the main characteristic is the ability to learn by examples and model complex non-linear relationships amongst these examples [48]. The ANNs basically operate in two phases:

- Training/Learning phase: The ANN receives raw data, (a finite set of information, examples about a particular problem or situation) as input, transform it into an appropriate internal representation (features vector) and use it to automatically learn the main patterns of that better represents input data;
- Operating phase: The ANN extrapolates the knowledge acquired during the learning process and is able to respond to new situations that are similar to the ones presented in the training.

In order to learn the representation of the information present in the raw data the ANNs use a hierarchical learning (layers of learning) approach. Therefore, the neural networks are composed of several inter-connected hidden layers of non-linear parameterized processing units (neurons) that have trainable parameters. Starting from the input layer, that receives the input signal (raw data), each successive hidden layer transforms the signal, via its neurons, and with the number of enough parameterized transformations, the network can learn to represent very complex non-linear relationships in the inputs [49–51].

Since the quantity of hidden layers and neurons defines the number of parameterized transformations an input signal encounters as it propagates through the network, the number of hidden layers and neurons is an important aspect when designing an ANN, considering that it can determine the learning capacity of the ANN. Thus, there is a substantial difference in learning capacity between DNNs, which are ANNs architectures with many neurons and hidden layers, and the Shallow Neural Networks (SNNs), which are ANNs architectures with few neurons and hidden layers. Generally, the DNNs have more than one hidden layer (usually between 2 and 10), and have the ability to representing and learning complex functions far more efficiently than the SNNs, that have only one hidden layer [38,49–51].

Furthermore, one of the main aspects of DNNs is the non-linear and differentiable activation function utilized to activate the neurons of the hidden layers, since without this type of function the network would be able to work only with linear problems. For a long time, the sigmoid functions (as the logistic sigmoid) were the most used activation functions option, including for DNNs architectures as the MLP (also called Deep Feedforward Neural Networks (DFNN)). However, in the literature it was pointed out a problem with this approach: DNNs with more than four hidden layers whose implement sigmoid functions tend to present a suffered performance, converging more slowly and apparently towards ultimately poorer local minima [52].

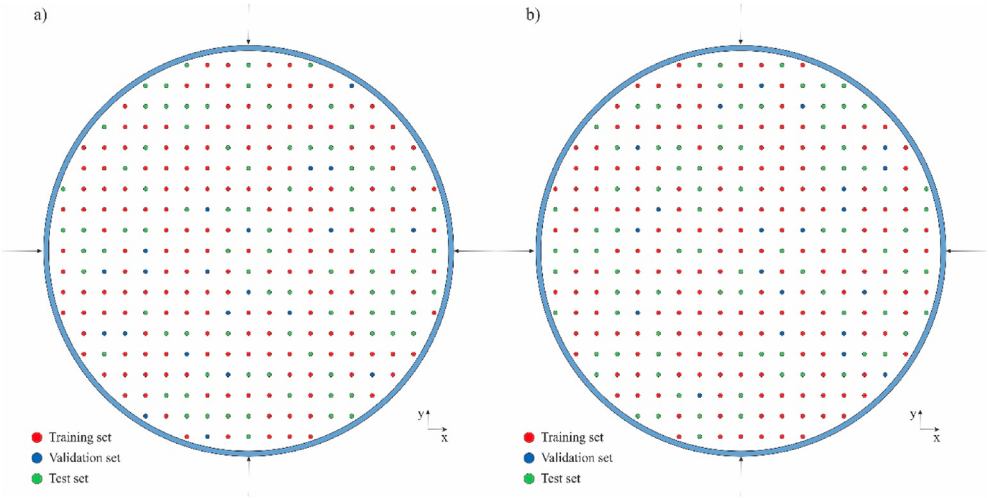

Fig. 2. Patterns used in Training, Validation and Test sets: a) slice where z = 0 cm; b) slice where z = −25 cm.

Table 1
Metrics used in order to evaluate the DRNN results.

Metrics	Equations
RE (%)	$\left(\frac{P_{true} - P_{ANN}}{P_{true}}\right) \times 100$
AE	$\lvert P_{true} - P_{ANN} \rvert$
MSE	$\frac{1}{N}\sum_{i=1}^{N}(P_{true} - P_{ANN})^2$
MAE	$\frac{1}{N}\sum_{i=1}^{N}\lvert P_{true} - P_{ANN} \rvert$
RMSE	$\sqrt{\frac{\sum_{i=1}^{N}(P_{true} - P_{ANN})^2}{N}}$

Due to this, a novel DNN architecture was proposed replacing the sigmoid functions for rectifier linear functions, thus receiving the name of Deep Rectifier Neural Network (DRNNs) [46]. The results of these experiments showed that DRNNs have a better performance than sigmoid activated DNNs, in such a way that the authors consider it to be a new milestone in the performance of DNNs when applied to supervised learning problems [46]. Recent cases in the literature, including ones in the nuclear areas, further demonstrated that the DRNN is a DNN model superior, in precision and training time, when compared with traditional MLPs activated with sigmoid functions [43–45,53] in a supervising learning task.

Therefore, considering the aspects pointed, the DNN model selected to deal with RPT tracking problem presented in this study was the DRNN.

3. Methodology

3.1. Radioactive particle tracking simulated system

The RPT system simulated with the MCNPX code [47] consists of a polyvinyl chloride (PVC) mixer, six 2″x2″ NaI(Tl) detectors and a radioactive particle. The mixer has 20 cm of diameter, 55 cm of length and it is filled with concrete made with Portland cement (density = 2.3 g cm^{-3}). The weight fractions of the concrete are available in the MCNPX compendium of materials [54]. The radioactive particle used in this study is a 662 keV point source with isotropic emission of gamma rays, representing ^{137}Cs radioisotope. In the simulations, the radioactive particle was placed in 3516 different positions within the mixer. Outside of the mixer, the detectors were placed in two planes (P1 and P2) perpendicular to the z-axis and the distance between these planes is 25 cm. Fig. 1 represents the simulated geometry.

In Fig. 1, "Ω" represents solid angle of the NaI(Tl) detectors. Upper plane (P1) has three detectors placed making a 120° angle between each other. Same detector distribution occurs for lower plane (P2). The distance between the detectors and the mixer is 20 cm. The simulated detectors are considered a homogeneous cylinder [55,56] and they consist of a NaI(Tl) crystal, surrounded by a reflective layer composed by magnesium oxide (MgO) and an outer aluminum (Al) layer, similarly to previous study [24].

In the MCNPX code input file, for calculations purposes, it is necessary to describe all the materials, with information such as density and weight fractions, and these information are available in the compendium of materials [54]. In the output file of the MCNPX code, tally card F8 gives the simulation response that represents the pulse height distribution (PHD) in each detector. The PHD was divided in 80 channels and each one has 10 keV of energy. The 67th channel corresponds to the photoelectric absorption region (photopeak), which is the area of interest in this study. In order to ensure that the relative error remains below 3% in the photopeak of all detectors, 3E8 number of histories (NPS) was chosen. The results of the MCNPX code were normalized to the source activity in the number of photons. It is worth mentioning that detection efficiency is considered the same in all detectors. The counts registered in the photopeak region were used in order to train the DRNN, however energy resolution was not considered in this study.

3.2. Location algorithm based on deep rectifier neural network

3.2.1. Dataset preparation

Using the simulated RPT system described in section 3.1, a dataset containing 3516 patterns was developed in the MCNPX code. Each pattern is formed by six inputs features representing the photopeak region of six detectors and three outputs targets corresponding to the radioactive particle instantaneous positions (x,y,z) within the mixer. Moreover, in these radioactive particle positions, the x, y and z coordinates range are, respectively, from −9 to 9 cm, −9 to 9 cm (both with a step of 1 cm) and −40 to 15 cm with a step of 5 cm.

In order to realize the experiments with the DRNN models the original dataset was divided into three subsets: training and

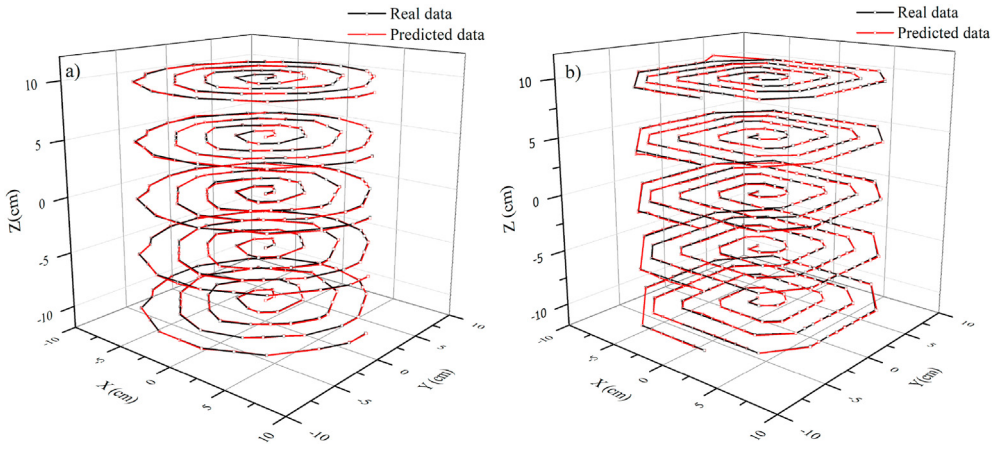

Fig. 3. 3D trajectories inside the mixer: a) spiral; b) square spiral.

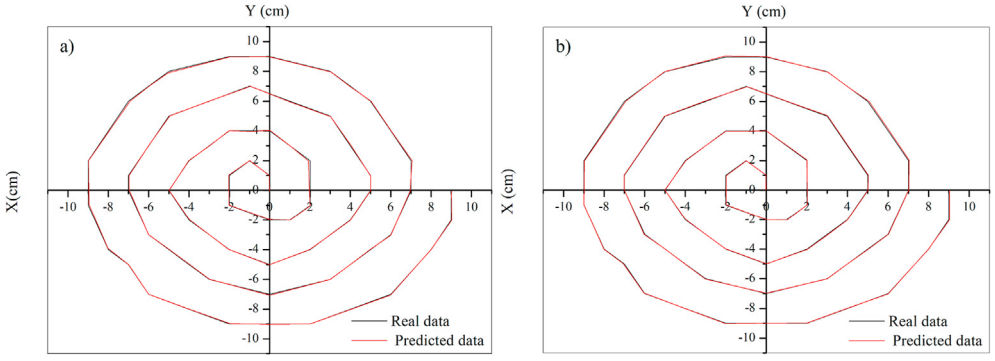

Fig. 4. Slices of spiral trajectory: a) z = −40 cm; b) z = −25 cm.

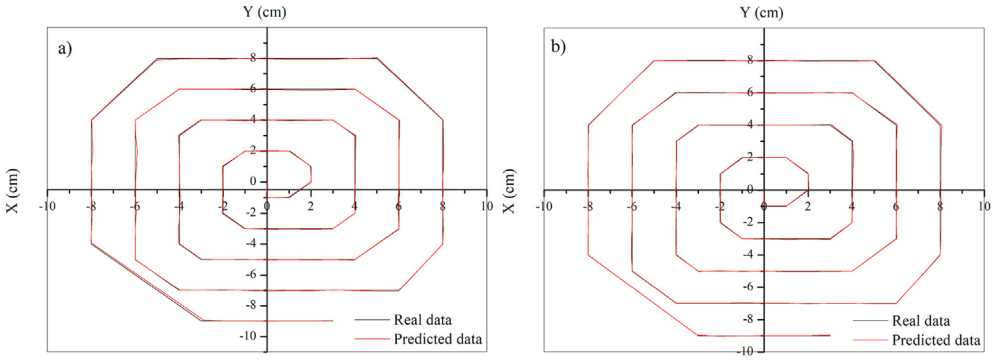

Fig. 5. Slices of square spiral trajectory: a) z = −40 cm; b) z = −25 cm.

Table 2
DRNN metrics using training, validation and test sets.

Metrics	Coordinates		
	X	Y	Z
MAE	0.02314	0.01898	0.03642
MSE	0.00094	0.00064	0.00586
RMSE	0.03064	0.02523	0.07653
R^2	0.99996	0.99997	0.99998

Table 3
DRNN metrics using test set.

Metrics	Coordinates		
	X	Y	Z
MAE	0.02642	0.02156	0.05304
MSE	0.00130	0.00086	0.01588
RMSE	0.03601	0.02927	0.12602
R^2	0.99994	0.99996	0.99995

validation sets, to be used during the learning phase of the network, and a test set, to evaluate the performance DRNN in the operation phase. Learning phase consists of, approximately, 60% (Training set) and 10% (Validation set) of the original dataset and operation phase

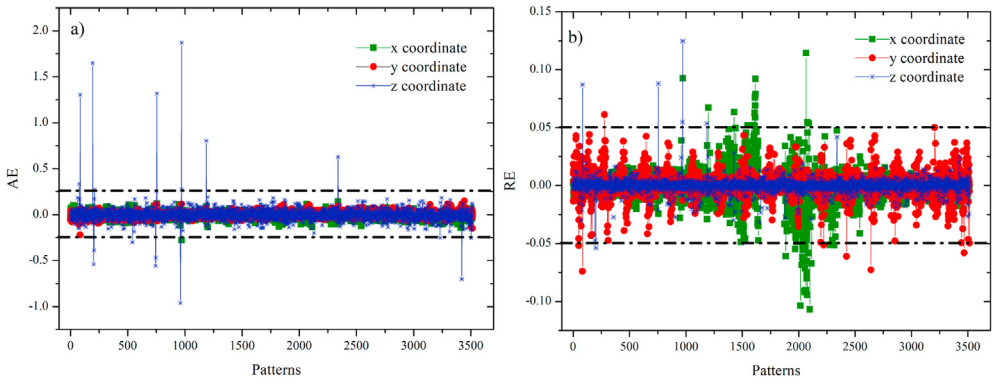

Fig. 6. Metrics: a) Absolute Error; b) Relative Error.

(Test set) consists of the remaining 30% of the original set. Fig. 2 shows slices of the RPT system, where z = 0 cm and z = −25 cm, in order to highlight patterns used in Training, Validation and Test sets.

Furthermore, to improve the performance of the DRNNs in the learning phase, the data patterns have been normalized according to Equation (1).

$$X_N = \frac{(X - X')}{S} \tag{1}$$

Where X_N is the normalized value; X is the original value; X' is the average and S is the standard deviation.

3.2.2. The DRNN model design process

Currently, a great part of the work in designing an ANN, as the DRNN, for a specific case is based on the specialist knowledge, taking in the account factors as the type of the problem (classification, regression, and forecasting) and the dataset characteristics (number of patterns for training and testing, the number of input features and output targets). Usually, the specialist, via a trial and error approach, manually defines the best hyperparameters (such as the number of layers, the number of neurons in each layer, and the activation function) for an ANN for the specific problem. Therefore, one of the main challenges when working with ANNs is the definition of hyperparameters. Due to this, some researches have been studying automated methods for this hyperparameters search task as: Random Search [57]; Robust Design of Artificial Neural Networks (RDANN) [58] and Bayesian optimization [59–61].

Therefore, in this study, the Bayesian optimization method was utilized to improve the process of design a DRNN for the RPT tracking problem. In order to implement the method, the Python hyperparameter optimization library Hyperas [62] was used and the following set of hyperparameters and their ranges were defined for the automated search process:

- Number of Hidden Layers: from 1 to 10 with a step of 1;
- Number of Neurons in the Hidden Layers: from 100 to 1000 with a step of 100;
- Hidden Layers Activation Function: Rectified linear unit (ReLu) [52] or Exponential linear unit (Elu) [63].

Other hyperparameters were defined manually:

- Optimizer: Adam [64];
- Error Function: Mean Squared Error (MSE);
- Number of Epochs: 4000;
- Batch Size: 32.

As a result of this process, a DRNN model with following characteristics achieved the smallest MSE in the test set:

- Number of Hidden Layers: 4;
- Number of Neurons in the Hidden Layers: [300, 300, 900, 1000];
- Hidden Layers Activation Function: [Elu, Elu, Elu, Elu].

Mathematical evaluation of the DRNN results will be made through well-known metrics such as Relative Error (RE), Absolute Error (AE), MSE, Mean Absolute Error (MAE) and Root Mean Squared Error (RMSE). Definition of the metrics are in Table 1. It is important to note that, in the following equations, N is the number of data, P_{true} is the real value given by MCNPX code and P_{ANN} is the predicted value by the ANN.

4. Results and discussions

In this section, the results achieved with the six layers DRNN (6-DRNN) model, described in section 3.2, for the RPT tracking problem, represented by the dataset defined in section 3.1, are presented. One of the possibilities when using RPT technique in mixers is to track the radioactive particle trajectory in order to evaluate how the flow is homogenized inside the mixer. Two 3D trajectories of the radioactive particle were tracked inside the mixer as follows Fig. 3. In both trajectories, it is possible to compare real data (simulated) with predicted data (6-DRNN).

In order to complement the view of real data and predicted data, Fig. 3a and b were sliced along z-axis. Two slices of each trajectory are shown in Fig. 4 and Fig. 5.

It is possible to observe, in Figs. 3, Figs. 4 and 5, that predicted data follows real data almost perfectly, which means that the location algorithm based on deep learning has a great precision in RPT tracking problems.

On this basis, to exemplify mathematically the performance of the DRNN, Table 2 presents the metrics using training, validation and test sets, which contains 3516 patterns. The results of the following metrics indicates the good convergence of the DRNN in this RPT system. Moreover, R^2 is the regression coefficient and its results indicate that predicted coordinates values are close to real values.

Since the test set contains patterns that were not included in the learning phase of the ANN models, it makes the ideal choice to evaluate the generalization capability of these models. In this way, Table 3 shows the performance of the DRNN on the test set, which contains 1055 patterns.

When observing the metrics from test set and learning phase (training and validation sets) it is possible to note that the results

are similar, which indicates that the DRNN was capable of generalize the knowledge acquired during the learning phase.

Aiming to visualize the behavior of the metrics along the entire dataset (3516 patterns), Fig. 6 shows AE and RE. It is possible to observe that most of the patterns, for x, y and z coordinates, are around ±0.025 of RE. Furthermore, the patterns are between −1.0 and 2.0 of AE, meanwhile the patterns are between −0.15 and 0.15 of RE. These results show that, in the most of the patterns, the errors are close to zero (the acceptable error range is delimited by black lines) and it shows how accurate the DRNN model can be in a RPT tracking system.

5. Conclusions

This study proposes the use of a novel RPT algorithm based on a deep learning model, more specifically a 6-layer deep rectifier neural network (DRNN). This algorithm was applied in a simulated test section that represents a simplified model of a mixer surrounded by six NaI(Tl) detectors in order to predict the radioactive particle position (x, y, z). Simulations were carried out using MCNPX code, which is based on Monte Carlo method, enabling the determination of an appropriate detection system in the early phase of the research. The results achieved by the DRNN presents RMSE for x, y and z coordinated, respectively, 0.03064, 0.02523 and 0.07653. The results of the metrics showed the great accuracy of the DRNN, which makes it a great tool in order to evaluate RPT tracking systems.

Declaration of competing interest

The authors declare that they have no known competing financial interests or personal relationships that could have appeared to influence the work reported in this paper.

Acknowledgments

The authors gratefully acknowledge scholarships from the Coordenação de Aperfeiçoamento de Pessoal de Nível Superior - Brasil (CAPES) - Finance Code 001, and the Conselho Nacional de Desenvolvimento Científico e Tecnológico - Brasil (CNPq). Thanks also to Instituto de Engenharia Nuclear (IEN).

References

[1] M.S. Abouelwafa, S.M. Kendall, The measurement of component ratios in multiphase systems using gamma-ray attenuation, J. Phys. E Sci. Instrum. 13 (1980) 341–345.
[2] Y. Mi, M. Ishii, L.H. Tsoukalas, Vertical two-phase flow identification using advanced instrumentation and neural networks, Nucl. Eng. Des. 184 (1998) 409–420.
[3] R. Hanus, L. Petryka, M. Zych, Velocity measurement the liquid–solid flow in vertical pipeline using gamma-ray absorption and weighted cross-correlation, Flow Meas. Instrum. 40 (2014) 58–63.
[4] R. Hanus, M. Zych, M. Kusy, M. Jaszczur, L. Petryka, Identification of liquid-gas flow regime in a pipeline using gamma-ray absorption technique and computational intelligence methods, Flow Meas. Instrum. 60 (2018) 17–23.
[5] G.H. Roshani, E. Nazemi, M.M. Roshani, A novel method for flow pattern identification in unstable operational conditions using gamma ray and radial basis function, Appl. Radiat. Isot. 123 (2017) 60–68.
[6] M. Zych, R. Hanus, B. Wilk, L. Petryka, D. Świsulski, Comparison of noise reduction methods in radiometric correlation measurements of two-phase liquid-gas flows, Measurement 129 (2018) 288–295, https://doi.org/10.1016/j.measurement.2018.07.035.
[7] V. Mosorov, M. Zych, R. Hanus, D. Sankowski, A. Saoud, Improvement of flow velocity measurement algorithms based on correlation function and twin plane electrical capacitance tomography, Sensors 20 (2020) 306, https://doi.org/10.3390/s20010306.
[8] R. Hanus, M. Zych, R. Chorzępa, A. Golijanek-Jędrzejczyk, Investigations of the methods of time delay measurement of stochastic signals using cross-correlation with the hilbert transform, in: IEEE 20th Mediterranean Electrotechnical Conference (MELECON), Palermo, Italy, vol. 2020, 2020, pp. 238–242, https://doi.org/10.1109/MELECON48756.2020.9140630.
[9] M. Khorsandi, S.A. Feghhi, Design and construction of a prototype gamma-ray densitometer for petroleum products monitoring applications, Measurement 44 (2011) 1512–1515.
[10] W.L. Salgado, R.S.F. Dam, C.M. Barbosa, A.X. Silva, C.M. Salgado, Monitoring system of oil by-products interface in pipelines using the gamma radiation attenuation, Appl. Radiat. Isot. 160 (2020), https://doi.org/10.1016/j.apradiso.2020.109125.
[11] A.A. Abdulrahman, E.M. Shokir, Artificial neural networks modeling for hydrocarbon gas viscosity and density estimation, J. King Saud Univ. - Eng. Sci. 23 (2011) 123–129.
[12] C.M. Salgado, L.E.B. Brandão, C.C. Conti, W.L. Salgado, Density prediction for petroleum and derivatives by gamma-ray attenuation and artificial neural networks, Appl. Radiat. Isot. 116 (2016) 143–149.
[13] G.H. Roshani, R. Hanus, A. Khazaei, M. Zych, E. Nazemi, V. Mosorov, Density and velocity determination for single-phase flow based on radiotracer technique and neural networks, Flow Meas. Instrum. 61 (2018) 9–14.
[14] J.S. Lin, M.M. Chen, B.T. Chao, A novel radioactive particle tracking facility for measurement of solids motion in gas fluidized beds, AIChE J. 31 (3) (1985) 465–473.
[15] F. Larachi, G. Kennedy, J. Chaouki, A gamma-ray detection system for 3-D particle tracking in multiphase reactors, Nucl. Instrum. Methods Phys. Res. Sect. A Accel. Spectrom. Detect. Assoc. Equip. 338 (2–3) (1994) 568–576.
[16] L. Godfroy F. Larachi, G. Kennedy, B. Grandjean, J. Chaouki, On-line flow visualization in multiphase reactors using neural networks, Appl. Radiat. Isot. 48 (1997) 225–235.
[17] S. Bhusarapu, M.H. Al-Dahhan, M.P. Dudukovic, S. Trujillo, T.J. O'Hern, Experimental study of the solids velocity field in gas–solid risers, Ind. Eng. Chem. Res. 44 (25) (2005) 9739.
[18] N. Devanathan, D. Moslemian, M.P. Dudukovic, Flow mapping in bubble columns using CARPT, Chem. Eng. Sci. 45 (1990) 2285–2291.
[19] S. Azizi, A. Yadav, Y.M. Lau, U. Hampel, S. Roy, M. Schubert, On the experimental investigation of gas-liquid flow in bubble columns using ultrafast X-ray tomography and radioactive particle tracking, Chem. Eng. Sci. 170 (2017) 320–331, https://doi.org/10.1016/j.ces.2017.02.015.
[20] M.A.S.M. Yunos, M.D.A. Usang, H. Ithnin, S.A. Hussain, H.M. Yusoff, S. Sipaun, Reconstruction algorithm of calibration map for RPT techniques in quadrilateral bubble column reactor using MCNPX code, European Journal of Engineering Research and Science 3 (1) (2018).
[21] M.A.S.M. Yunos, S.A. Hussain, S.M. Sipaun, Industrial radiotracer application in flow rate measurement and flowmeter calibration using ^{99m}Tc and ^{198}Au nanoparticles radioisotope, Appl. Radiat. Isot. 143 (2019) 24–28.
[22] A. Yadav, T.K. Gaurav, H.J. Pant, S. Roy, Machine Learning Based Position-rendering Algorithms for Radioactive Particle Tracking Experimentation, American Institute of Chemical Engineers, 2020, https://doi.org/10.1002/aic.16954.
[23] L. Spreutels, B. Haut, R. Legros, F. Bertrand, J. Chaouki, Experimental investigation of solid particles flow in a conical spouted bed using radioactive particle tracking, AIChE J. 62 (2015) 26–37.
[24] R.S.F. Dam, T.P. Teixeira, W.L. Salgado, C.M. Salgado, A new application of radioactive particle tracking using MCNPX code and artificial neural network, Appl. Radiat. Isot. 149 (2019) 38–47.
[25] R.S.F. Dam, C.M. Barbosa, J.M. Lopes, J.L. Thalhofer, L.B. Silva, C.M. Salgado, A.X. Silva, Radioactive particle tracking methodology to evaluate concrete mixer using MCNPX code, Radiat. Phys. Chem. 160 (2019) 26–29.
[26] J. Chaouki, F. Larachi, P. Dudukovic, Non-Invasive Monitoring of Multiphase Flows, Elsevier Science B.V., Amsterdam, The Netherlands, 1997.
[27] V. Blet, P. Berne, S. Legoupil, et al., Radioactive tracing as aid for diagnosing chemical reactors, Oil and Gas Science and Technology – Rev. IFP. 55 (2) (2000) 171–183.
[28] J. Doucet, F. Bertrand, J. Chaouki, An extended radioactive particle tracking method for systems with irregular moving boundaries, Powder Technol. 181 (2) (2008) 195–204.
[29] V. Mosorov, J. Abdullah, MCNP5 code in radioactive particle tracking, Appl. Radiat. Isot. 69 (2011) 1287–1293.
[30] C.M. Salgado, L.E.B. Brandão, C.M.N.A. Pereira, R. Schirru, R. Ramos, A.X. Silva, Prediction of volume fractions in three-phase flows using nuclear technique and artificial neural network, Appl. Radiat. Isot. 67 (2009) 1812–1818.
[31] C.M. Salgado, C.M.N.A. Pereira, R. Schirru, L.E.B. Brandão, Flow regime identification and volume fraction prediction in multiphase flows by means of gamma-ray attenuation and artificial neural networks, Prog. Nucl. Energy 52 (6) (2010) 555–562.
[32] G.H. Roshani, A. Karami, A. Salehizadeh, E. Nazemi, The capability of radial basis function to forecast the volume fractions of the annular three-phase flow of gas-oil-water, Appl. Radiat. Isot. 129 (2017) 156–162.
[33] R.R.W. Affonso, R.S.F. Dam, W.L. Salgado, A.X. Silva, C.M. Salgado, Flow regime and volume fraction identification using nuclear techniques, artificial neural networks and computational fluid dynamics, Appl. Radiat. Isot. 159 (2020) 109103, https://doi.org/10.1016/j.apradiso.2020.109103.
[34] C.M. Salgado, R.S.F. Dam, W.L. Salgado, R.R.W. Affonso, C.M.N.A. Pereira, R. Schirru, The comparison of different multilayer perceptron and General Regression Neural Networks for volume fraction prediction using MCNPX code, Appl. Radiat. Isot. 162 (2020), https://doi.org/10.1016/j.apradiso.2020.109170.
[35] W.L. Salgado, R.S.F. Dam, T.P. Teixeira, C.C. Conti, C.M. Salgado, Application of

artificial intelligence in scale thickness prediction on offshore petroleum using a gamma-ray densitometer, Radiat. Phys. Chem. 168 (2020) 108549, https://doi.org/10.1016/j.radphyschem.2019.108549.
[36] G.H. Roshani, E. Nazemi, Intelligent densitometry of petroleum products in stratified regime of two phase flows using gamma ray and neural network, Flow Meas. Instrum. 58 (2017) 6–11.
[37] C.M.N.A. Pereira, R. Schirru, K.J. Gomes, J.L. Cunha, Artificial Neural Networks for Radiation Dose Prediction in Nuclear Emergencies: Preliminary Investigations. Advances in Computer Science Research, Atlantis Press ISSN, 2016, https://doi.org/10.2991/msota-16.2016.98, 2352–538X.
[38] R.K. Srivastava, K. Greff, J. Schmidhuber, Training Very Deep Networks. The Swiss AI Lab IDSIA/USI/SUPSI, Neural Information Processing Systems, NIPS), 2015.
[39] M. Gheisari, G. Wang, M.Z.A. Bhuiyan, A survey on deep learning in big data, in: IEEE International Conference on Computational Science and Engineering (CSE) and IEEE International Conference on Embedded and Ubiquitous Computing, EUC), Guangzhou, 2017, pp. 173–180.
[40] F. Chen, M.R. Jahanshahi, NB-CNN, Deep learning-based crack detection using convolutional neural network and naïve bayes data fusion, in: IEEE Transactions on Industrial Electronics, vol. 65, 2018, pp. 4392–4400, https://doi.org/10.1109/TIE.2017.2764844, 5.
[41] F.D.S. Ribeiro, F. Calivà, D. Chionis, A. Dokhane, A. Mylonakis, C. Demazière, G. Leontidis, S.D. Kollias, Towards a deep unified framework for nuclear reactor perturbation analysis, in: IEEE Symposium Series on Computational Intelligence, SSCI), Bangalore, India, 2018, pp. 120–127, https://doi.org/10.1109/SSCI.2018.8628637.
[42] F. Calivá, F.D.S. Ribeiro, A. Mylonakis, C. Demazière, P. Vinai, G. Leontidis, S. Kollias, A deep learning approach to anomaly detection in nuclear reactors, in: International Joint Conference on Neural Networks, IJCNN), Rio de Janeiro, 2018, pp. 1–8, https://doi.org/10.1109/IJCNN.2018.8489130.
[43] F.S.M. Desterro, M.C. Santos, K.J. Gomes, A. Heimlich, R. Schirru, C.M.N.A. Pereira, Development of a Deep Rectifier Neural Network for dose prediction in nuclear emergencies with radioactive material releases, Prog. Nucl. Energy 118 (2020), https://doi.org/10.1016/j.pnucene.2019.103110.
[44] M.C. Santos, V.H.C. Pinheiro, F.S.M. Desterro, R.K. Avellar, R. Schirru, A.S. Nicolau, A.M.M. Lima, Deep rectifier neural network applied to the accident identification problem in a PWR nuclear power plant, Ann. Nucl. Energy 133 (2019) 400–408.
[45] V.H. Pinheiro, M.C. Santos, F.S.M. Desterro, R. Schirru, C.M.N.A. Pereira, Nuclear Power Plant accident identification system with “don’t know” response capability: novel deep learning-based approaches, Ann. Nucl. Energy 137 (2020), https://doi.org/10.1016/j.anucene.2019.107111.
[46] X. Glorot, A. Bordes, Y. Bengio, Deep sparse rectifier neural networks. Proceedings of the fourteenth international conference on artificial intelligence and statistics, in: PMLR, vol. 15, 2011, pp. 315–323.
[47] D.B. Pelowitz, MCNPX TM User's Manual. Version 2.5.0, Los Alamos National Laboratory, 2005. LA-CP-05-0369.
[48] S. Haykin, Neural Networks, A Comprehensive Foundation, second ed., Prentice Hall, 1999.
[49] J. Schmidhuber, Deep learning in neural networks: an overview, Neural Netw. Off. J. Int. Neural Netw. Soc. 61 (2015) 85–117.
[50] Y. LeCun, Y. Bengio, G. Hinton, Deep learning, Nature 521 (2015) 436–444.
[51] B.B. Benuwa, Y.Z. Zhan, B. Ghansah, D.K. Wornyo, F.B. Kataka, A review of deep machine learning, Int. J. Eng. Res. Afr. 24 (2016) 124–136. https://doi.org/10.4028/www.scientific.net/JERA.24.124.
[52] X. Glorot, Y. Bengio, Understanding the difficulty of training deep feedforward neural networks, in: Proc. AISTATS, vol. 9, 2010, pp. 249–256.
[53] D. Pedamonti, Comparison of Non-linear Activation Functions for Deep Neural Networks on MNIST Classification Task, CoRR - Computing Research Repository, 2018.
[54] R.J. McConn Jr., C.J. Gesh, R.A. Rucker, R.G. Williams II, Compendium of Material Composition Data for Radiation Transport Modeling, Pacific Northwest National Laboratory, 2011. PNNL-15870, Rev. 1.
[55] M.J. Berger, S.M. Seltzer, Response functions for sodium iodide scintillation detectors, Nucl. Instrum. Methods 104 (1972) 317–332.
[56] C.M. Salgado, L.E.B. Brandão, R. Schirru, C.M.N.A. Pereira, C.C. Conti, Validation of aNaI(Tl) detector's model developed with MCNP-X code, Prog. Nucl. Energy 59 (2012) 19–25.
[57] J. Bergstra, Y. Bengio, Random search for hyper-parameter optimization, J. Mach. Learn. Res. 13 (2012) 281–305.
[58] J.M. Ortiz-Rodriguez, M.R. Martinez-Blanco, J.M. Varamontes, H.R. Vega-Carrillo, Robust design of artificial neural networks methodology in neutron spectrometry, in: K. Prof Suzuki (Ed.), Artificial Neural Networks - Architectures and Application, s, 2013.
[59] J. Snoek, H. Larochelle, R. Adams, Practical Bayesian optimization of machine learning algorithms, in: Advances in Neural Information Processing Systems, vol. 25, 2012, pp. 2960–2968.
[60] I. Dewancker, M. McCourt, S. Clark, Bayesian Optimization for Machine Learning: A Practical Guidebook, SigOpt, San Francisco, CA 94108, 2015 arXiv:1612.04858.
[61] B. Shahriari, K. Swersky, Z. Wang, R.P. Adams, N. Freitas, Taking the human out of the loop: a review of bayesian optimization, in: Proceedings of the IEEE, vol. 104, 2016, pp. 148–175, 1.
[62] M. Pumperla, Hyperas: a Very Simple Convenience Wrapper Around Hyperopt for Fast Prototyping with Keras Models, 2017. https://maxpumperla.com/hyperas/. (Accessed 1 June 2020).
[63] D.A. Clevert, T. Unterthiner, S. Hochreiter, Fast and accurate deep network learning by exponential linear units (elus), ICLR, 2015 arXiv:1511.07289.
[64] D.P. Kingma, J. Ba, Adam, A method for stochastic optimization, in: 3rd International Conference for Learning Representations, San Diego, 2015 arXiv:1412.6980.